The endocannabinoid 2-AG controls skeletal muscle cell differentiation via CB1 receptor-dependent inhibition of K_v7 channels

Fabio A. Iannotti[a], Cristoforo Silvestri[a], Enrico Mazzarella[a], Andrea Martella[a], Daniela Calvigioni[b,c], Fabiana Piscitelli[a], Paolo Ambrosino[d], Stefania Petrosino[a], Gabriella Czifra[e], Tamás Bíró[e], Tibor Harkany[b,c], Maurizio Taglialatela[d], and Vincenzo Di Marzo[a,1]

[a]Endocannabinoid Research Group, Institute of Biomolecular Chemistry, National Council of Research (Consiglio Nazionale delle Ricerche), 80078 Pozzuoli, Italy; [b]Department of Medical Biochemistry and Biophysics, Karolinska Institutet, SE-17177 Stockholm, Sweden; [c]Department of Molecular Neurosciences, Center for Brain Research, Medical University of Vienna, A-1090 Vienna, Austria; [d]Department of Medicine and Health Sciences, University of Molise, 86100 Campobasso, Italy; and [e]Department of Physiology and Cell Physiology Research Group of the Hungarian Academy of Sciences, University Medical School of Debrecen, 4032, Debrecen, Hungary

Edited by Leslie Lars Iversen, University of Oxford, Oxford, United Kingdom, and approved May 6, 2014 (received for review April 14, 2014)

Little is known of the involvement of endocannabinoids and cannabinoid receptors in skeletal muscle cell differentiation. We report that, due to changes in the expression of genes involved in its metabolism, the levels of the endocannabinoid 2-arachidonoylglycerol (2-AG) are decreased both during myotube formation in vitro from murine C_2C_{12} myoblasts and during mouse muscle growth in vivo. The endocannabinoid, as well as the CB1 agonist arachidonoyl-2-chloroethylamide, prevent myotube formation in a manner antagonized by CB1 knockdown and by CB1 antagonists, which, per se, instead stimulate differentiation. Importantly, 2-AG also inhibits differentiation of primary human satellite cells. Muscle fascicles from CB1 knockout embryos contain more muscle fibers, and postnatal mice show muscle fibers of an increased diameter relative to wild-type littermates. Inhibition of $K_v7.4$ channel activity, which plays a permissive role in myogenesis and depends on phosphatidylinositol 4,5-bisphosphate (PIP2), underlies the effects of 2-AG. We find that CB1 stimulation reduces both total and $K_v7.4$-bound PIP2 levels in C_2C_{12} cells and inhibits $K_v7.4$ currents in transfected CHO cells. We suggest that 2-AG is an endogenous repressor of myoblast differentiation via CB1-mediated inhibition of $K_v7.4$ channels.

The endocannabinoid system (ECS) refers to a large group of endogenous molecules including the two major arachidonate-derived neuromodulatory mediators, anandamide (AEA) and 2-arachidonoylglycerol (2-AG), known as endocannabinoids (EC); several enzymes involved in the metabolism of AEA (NAPE-PLD, ABDH4, GDE1, PTPN22 for biosynthesis and FAAH for degradation) and 2-AG (DAGLα and DAGLβ for biosynthesis and MAGL, ABDH6, ABDH12, and FAAH for degradation); and two G protein-coupled receptors known as cannabinoid receptor of type-1 (CB1) and type-2 (CB2). AEA also activates the cation permeant transient receptor potential vanilloid type-1 (TRPV1) channels (1). In mammals, the ECS regulates a large number of physiological processes; alterations in its activity are in fact responsible for the onset or progression of many types of disorders affecting both the central and the peripheral nervous system as well as other organs (2–5). So far, a few studies have reported that CB1 receptor activity controls key skeletal muscle metabolic processes such as insulin signaling, glucose uptake, and fatty acid oxidation (6, 7). However, little, if anything at all, is known about the expression profile and the functional role played by the ECS during skeletal muscle development.

Skeletal myogenesis is a tightly regulated process that requires coordinated changes in a large number of genes allowing proliferating myoblasts to withdraw from the cell cycle and fuse to form large multinucleated myotubes (8). Several classes of ion channels play a pivotal role in the initiation of the differentiation process. For example, the sequential activation of two distinct classes of K^+ channels, the ether-a-go-go $K_v10.1$ and the inward-rectifier KIR2.1 (9, 10), is known to be one of the first molecular events that causes myoblast hyperpolarization. This event, in turn, leads to the activation of voltage-dependent T-type Ca^{2+} channels, which increase the $[Ca^{2+}]_i$ necessary to initiate myoblast commitment to differentiation into myotubes (11). More recently, members of the K_v7 (KCNQ) subfamily of voltage-activated K^+ channels have been found to be expressed in both myoblasts and myotubes (12, 13), and, in particular, it has been shown that $K_v7.4$ channel expression plays a permissive role in skeletal myogenesis (14).

The K_v7 subfamily comprises five subunits ($K_v7.1$–$K_v7.5$), each showing distinct tissue distribution and physiological properties. K_v7 channel function is regulated by several classes of $G_{q/11}$-coupled receptors including muscarinic (15), bradikynin (16), serotonin (17), and somatostatin receptors (18). Stimulation of these receptors leads to phospholipase C (PLC) activation and subsequent hydrolysis of phosphatidylinositol 4,5-bisphosphate (PIP2) into inositol 1,4,5-trisphosphate (IP3) and diacylglycerol (DAG). Thus, considering that PIP2 is strictly required for K_v7 channels activity, $G_{q/11}$-coupled receptor stimulation represents one of the most important cellular mechanisms through which this subclass of K^+ channels is kept under negative control (19). Interestingly, the M current, which is underlied by K_v7 channels,

Significance

Although CB1 cannabinoid receptors control skeletal muscle insulin signaling, little is known of their role in muscle formation during differentiation from myoblasts to myotubes. The voltage-dependent K_v7 K^+ channels, which are tonically activated by the membrane phospholipid phosphatidylinositol 4,5-bisphosphate (PIP2), instead activate myotube formation. We found that the levels of the endogenous CB1 agonist 2-arachidonoylglycerol are decreased during murine myoblast differentiation into myotubes, whereas CB1 expression is up-regulated. CB1 activation inhibits myotube formation. This effect is exerted by reducing PIP2 binding to $K_v7.4$, which represents the K_v7 subunit responsible for the pro-myogenic effects. Accordingly, CB1 activation inhibits $K_v7.4$-mediated currents in transfected CHO cells. The endocannabinoid system might thus play a role in skeletal muscle dystrophies.

Author contributions: F.A.I., C.S., and V.D. designed research; F.A.I., C.S., E.M., A.M., D.C., F.P., P.A., S.P., and G.C. performed research; F.A.I., T.B., T.H., M.T., and V.D. analyzed data; and F.A.I. and V.D. wrote the paper.

The authors declare no conflict of interest.

This article is a PNAS Direct Submission.

[1]To whom correspondence should be addressed. E-mail: vdimarzo@icb.cnr.it.

This article contains supporting information online at www.pnas.org/lookup/suppl/doi:10.1073/pnas.1406728111/-/DCSupplemental.

can be also inhibited following CB1 receptor stimulation by AEA at the postsynaptic level in hippocampal neurons (20) or by stimulation of the $G_{q/11}$-coupled orphan receptor GPR55 (21).

In this study, we have endeavored to understand the role played by the ECS in muscle development and its impact on K_v7 activity during myogenesis by using molecular biology, biochemical, pharmacological, morphological, and electrophysiological techniques. Our results indicate that the endocannabinoid 2-AG tonically inhibits differentiation of mouse and human myoblasts via sequential activation of CB1 receptors, reduction of PIP2 levels, and inhibition of K_v7 channel activity.

Results

Levels of AEA and 2-AG and mRNA Expression Profile of Genes Related to Their Metabolism During C_2C_{12} Cell Differentiation. To gain information about the tone of the ECS and its potential changes during in vitro myogenesis, we measured AEA and 2-AG levels in C_2C_{12} cells by liquid chromatography atmospheric pressure chemical ionization mass spectrometry (LC-APCI-MS) in myoblasts and after 3 and 7 d of their exposure to differentiation medium (DM). We found that, during myotube formation, AEA levels tended to decrease albeit not reaching statistical significance (Fig. 1*A*), whereas 2-AG levels strongly declined already after 3 d of myoblast exposure to DM and remained reduced up to at least day 7 of the differentiation program (Fig. 1*A*). To understand whether the changes in EC levels were due to changes in the mRNA expression of EC metabolic enzymes, we determined by quantitative PCR (qPCR) the mRNA expression profile for the entire set of genes known to encode for enzymes involved in EC synthesis (such as *Napepld*, *Abdh4*, *Gde1*, and *Ptpn22* for AEA or *Dagla* and *Daglb* for 2-AG) and degradation (such as *Faah* for AEA or *Magl*, *Abdh6*/*12*, and *Faah* for 2-AG) (Table S1). Our analysis revealed that during myotube formation the expression profile of genes involved in AEA metabolism was not significantly changed, except for *Ptpn22* and *Faah*, the mRNA transcript levels of which were slightly decreased in myotubes (Fig. 1*B*). In contrast, among the genes related to 2-AG metabolism, the expression of *Dagla* and *Abhd12* was slightly reduced (by less than twofold), whereas *Magl* expression was significantly up-regulated (by about twofold) during C_2C_{12} cell differentiation (Fig. 1*B*). Accordingly, Western blot analysis revealed that, concomitant to increased myosin heavy chain (MyHC) protein expression during C_2C_{12} cell differentiation, *Dagla* levels are not significantly changed, although a decreasing trend is observed at 72 h, whereas *Magl* levels increase steadily over time (Fig. 1*C*).

Potential changes in AEA and 2-AG levels were then evaluated in mouse muscle at different developmental stages. The *quadriceps femoris* muscle was dissected from the leg of mouse embryos or pups at embryonic day 18 (E18) or at postnatal days 4 and 14 (P4 and P14), and its purified lipid extract was subsequently subjected to LC-APCI-MS analysis. As shown in Fig. 1*D*, endogenous levels of AEA decreased by about fivefold from E18 to P4, but rebound by P14, whereas 2-AG levels remained constant at E18 and P4, but then decreased by about 50% at P14. Taken together, these results indicate that during muscle formation, both in vitro and in vivo, the endogenous levels of 2-AG decline with myotube formation and muscle growth, respectively.

CB1 and CB2 Expression Profile During Murine C_2C_{12} and Primary Human Skeletal Muscle Cell Differentiation. In our attempt to characterize the ECS and its role during skeletal muscle cell differentiation, the expression of transcripts from the *Cnr1* and *Cnr2* genes, encoding for CB1 and CB2 receptors, respectively, was also evaluated in C_2C_{12} myoblasts [in growth medium (GM)] and at different time points (1–3 d) during myotube formation [in differentiation medium (DM)], by qPCR. The results obtained show that *Cnr1* expression was already strong in proliferating myoblasts and further increased after 1 d of exposure to DM, reaching a plateau after 2 d (Fig. 2*A*). In contrast, *Cnr2* expression in myoblasts (GM) was much lower, and did not significantly increase after 1 d of exposure to DM; however, an increase in *Cnr2* mRNA levels was found after 2 d of cell exposure to DM, and this continued after 3 d (Fig. 2*A*). Likewise, in primary human skeletal muscle cells (hSkMC), we found that *CNR1* mRNA expression was increased by about eightfold after 2 d of myoblast exposure to DM. In contrast, *CNR2* gene expression was not modified (Fig. 2*B*). In C_2C_{12} cells, in keeping with the observed *Cnr1* and *Cnr2* mRNA expression profile, Western blot analysis showed a >4-fold increase in CB1 receptor expression, with much smaller effects on CB2 (Fig. 2*C*).

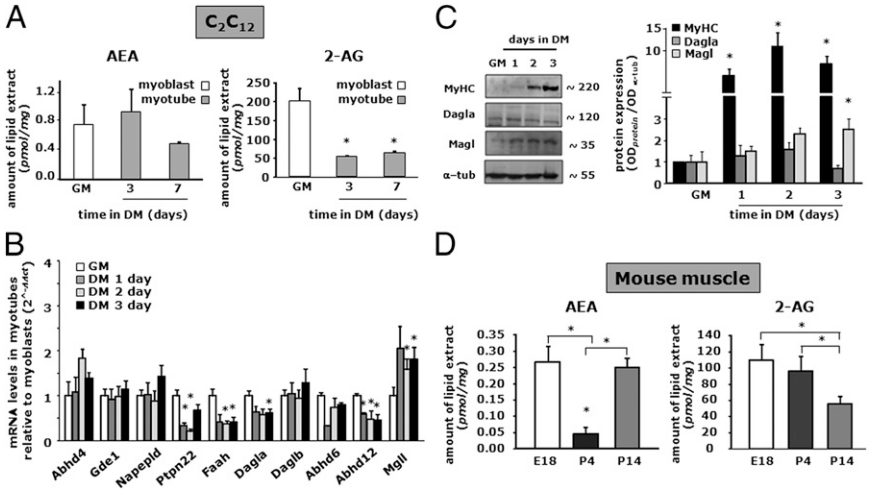

Fig. 1. Changes in AEA and 2-AG levels during C_2C_{12} cell differentiation. (*A* and *D*) Endogenous levels of AEA and 2-AG were quantified by LC-APCI-MS in C_2C_{12} myoblasts at day 0 (GM) and after 3 and 7 d of exposure to DM (*A*) or mouse quadriceps femoris at E18 and at 4 and 14 d after birth (P4, P14, respectively) (*D*). AEA and 2-AG levels are normalized to the total lipid amounts extracted from cells. (*B*) Relative mRNA expression profiles of genes involved in AEA and 2-AG metabolism during C_2C_{12} differentiation (up to 3 d) by qPCR analysis. (*C*) Western blot analysis (*Left*) and quantification (*Right*) of MyHC, *Dagla*, *Magl*, and α-tubulin protein expression in total lysates from C_2C_{12} myoblasts (GM) or cells exposed to DM for the indicated times. The quantification of the averaged OD values for the MyHC, *Dagla*, and *Magl* bands was normalized to that of α-tubulin. *$P \leq 0.05$ vs. the respective values in myoblasts (GM) or vs. the E18 group. Each data point was obtained from at least four independent determinations for each experimental condition.

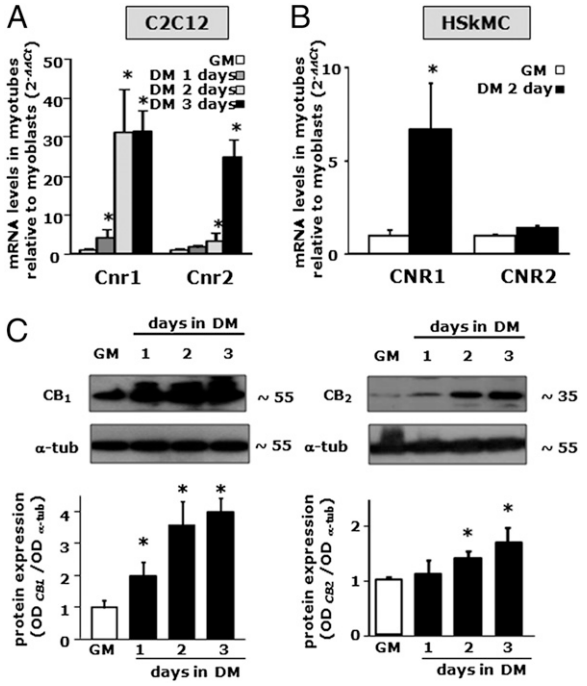

Fig. 2. CB1 and CB2 mRNA and protein expression profile during murine C_2C_{12} and hSkMC myotube formation. (*A* and *B*) qPCR analysis of *Cnr1* and *Cnr2* mRNA expression levels in C_2C_{12} (*A*) or hSkMC (*B*) in GM or exposed to DM for various amounts of time. Data are expressed as $2^{-\Delta\Delta Ct}$ relative to S16. $^*P < 0.05$ vs. myoblasts (GM). (*C*) Western blot analysis of CB1 and CB2 protein levels in differentiating C_2C_{12} cells. Representative blots showing the approximate molecular mass of each CB protein (expressed in kDa) (*Upper*) and quantification of the averaged OD values for CB1 and CB2 normalized to those of α-tubulin (*Lower*) are shown. $^*P \leq 0.05$ vs. respective myoblasts (GM). Each data point is from at least four independent determinations.

In conclusion, these findings indicate that both *Cnr1* and *Cnr2* genes are expressed in murine C_2C_{12} cells, with *Cnr1* being the most expressed and more rapidly up-regulated within the first 24–48 h of myotube formation. Down-regulation of *Cnr1* was instead observed in vivo in mice, for example, in the *quadriceps femoris*, during development from E18 to P4 (see below).

Effects of AEA, 2-AG, and Noladin Ether on the Early Phase of Myotube Formation. To clarify the biological significance of the changes described so far, C_2C_{12} myoblasts were induced to differentiate in the presence of exogenous AEA or 2-AG or of drugs able to selectively modulate EC levels or activity at receptors. After 1 d of exposure to DM (± drugs), total mRNA was isolated under each condition and analyzed by qPCR to examine the expression levels of specific skeletal muscle differentiation-related genes, such as myogenin (*Myog*), troponin T1 (*Tnnt-1*), and Krp1 (Sarcosin), which are normally up-regulated during myotube formation in C_2C_{12} cells (Fig. S1).

As shown in Fig. 3*A*, exogenous 2-AG (1–3 μM), but not AEA (1–3 μM), significantly inhibited *Myog* mRNA expression. However, considering that FAAH and MAGL are active also on synthetic AEA and 2-AG, we evaluated the effects of these exogenous ECs in the presence of selective DAGLα, FAAH, and MAGL inhibitors, i.e., OMDM188 (1 μM), URB567 (0.6–1 μM), and JZL184 (0.6–1 μM), respectively. Inhibiting endogenous 2-AG biosynthesis or degradation with OMDM188 and JZL184 (1 μM) per se slightly enhanced and reduced *Myog* transcript levels, respectively, suggesting the presence of an endogenous tone of 2-AG exerting an inhibitory effect on myogenesis (Fig. 3*B*). Indeed, exogenous 2-AG (3 μM) when provided to C_2C_{12} cells together with a noneffective dose of JZL184 (0.6 μM) produced a stronger inhibition of *Myog* expression (Fig. 3*B*). By contrast, exogenous AEA (1–3 μM) given alone or in combination with a noneffective dose of URB567 (0.6 μM) did not alter *Myog* mRNA expression. URB567 at 1 μM also produced no effect on *Myog* mRNA expression (Fig. 3*B*). Moreover, 2-arachidonylglyceryl ether (noladin ether), a nonhydrolyzable structural analog of 2-AG showing high affinity for CB1 (22, 23), inhibited in a more potent and dose-dependent manner (EC_{50} = 0.52 μM) the expression of *Myog* (Fig. 3*C*) as well as of *Tnnt-1* and *Krp1* mRNA (Fig. S2*A*).

In summary, activation of CB1 receptors with either exogenous or endogenously elevated (2-AG but not AEA) ECs, or a more enzymatically stable 2-AG analog, inhibits C_2C_{12} myoblast differentiation, whereas inhibition of 2-AG biosynthesis produces the opposite effect.

Pharmacological and Genetic Manipulation of CB1 and CB2 Receptors During C_2C_{12} Cell and Primary hSkMC Differentiation. To clarify the role played by CB1 and CB2 receptors in myogenesis, we exposed C_2C_{12} cells to DM for 24–72 h in the presence of selective CB1 or CB2 agonists or inverse agonists. Arachidonoyl-2-chloroethylamide (ACEA), a CB1 agonist selective against CB2 receptors (24), significantly reduced the mRNA expression levels of *Myog* in a dose (up to 3 μM) and time-dependent manner (up to 3 d of DM exposure) (Fig. 4 *A* and *B*). Also the mRNA expression levels of *Tnnt-1* and *Krp1* were reduced after C_2C_{12} cell exposure to ACEA (1–3 μM) (Fig. S2*B*).

A decrease in *Myog* mRNA expression was also found after 24 h of C_2C_{12} cell exposure to DM in the presence of the CB1/CB2 receptor agonist WIN 55,212–2 (up to 3 μM; EC_{50} = 0.68 μM) (Fig. S2*C*). Interestingly, SR141716 (rimonabant) and AM251, two selective antagonists/inverse agonists at CB1 receptors (25, 26), enhanced the mRNA expression levels of *Myog* in a dose-dependent manner (up to 3 μM; EC_{50} = ~0.8 μM for both drugs) (Fig. 4 *C* and *D*) as well as those of *Tnnt-1* (Fig. S2*C*) after 24 h of exposure. Finally, ACEA effects were counteracted by a noneffective dose of SR141716 (0.6 μM) (Fig. 4*E*).

Interestingly, also in hSkMCs, we found that *MYOG* and *TNNT1* transcript levels were reduced after 2 d of myoblast

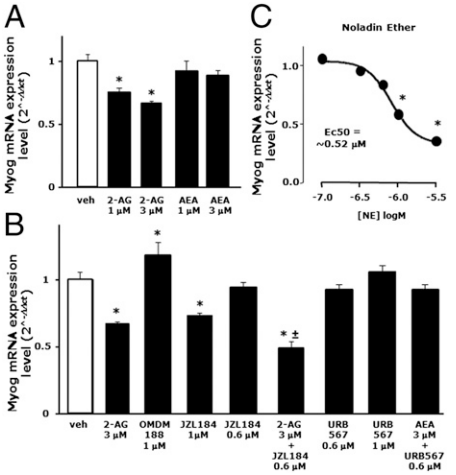

Fig. 3. Effect of AEA, 2-AG, and noladin ether on the early phase of myotube formation in C_2C_{12} cells. (*A* and *B*) Myogenin (*Myog*) mRNA expression levels were quantified by qPCR after exposure of C_2C_{12} cells to DM for 24 h in presence of vehicle (DMSO), 2-AG, AEA, OMDM188, JZL184, and/or URB567 at the indicated concentrations. Each bar represents the mean ± SEM of at least four separate experiments. (*C*) Concentration-response curve showing *Myog* mRNA expression levels in C_2C_{12} cells exposed to DM for 24 h in the presence of increasing concentrations of noladin ether.

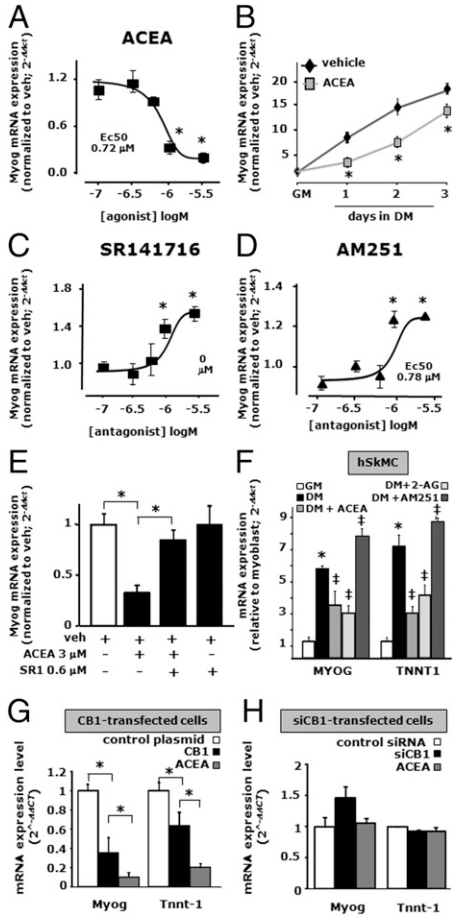

Fig. 4. Pharmacological and genetic manipulation of CB1 receptors during C_2C_{12} cell differentiation. (*A–D*) Myogenin (*Myog*) mRNA expression levels, as evaluated by qPCR, in C_2C_{12} cells exposed to DM for 24 h in the presence of increasing concentrations of ACEA (up to 3 μM, EC_{50} 0.72 μM) (*A*), in the presence of 1 μM of ACEA incubated for the indicated times (*B*) and in response to increasing concentrations of SR141716 (up to 3 μM, EC_{50} 0.82 μM) (*C*) or AM251 (up to 3 μM, EC_{50} 0.78 μM) (*D*). Each data point of the concentration-response curves represents the mean ± SEM of three to four separate determinations performed in quadruplicate. $^*P \leq 0.05$ vs. the lowest noneffective concentration (0.1 μM for each drug). (*E*) After 24 h of DM exposure, the inhibition effect of 3 μM of ACEA on *Myog* expression was prevented by SR141716 at the noneffective concentration of 0.6 μM. (*F*) Effect of ACEA (3 μM), 2-AG (3 μM), and AM251 (3 μM) on *MYOG* and *TNNT-1* expression levels in primary hSkMC after 48 h of exposure to DM. $^*P \leq 0.05$ vs. GM (+ veh); $^‡P \leq 0.05$ vs. DM (+veh). (*G* and *H*) mRNA expression levels of *Myog* and *Tnnt-1* in CB1 overexpressing (*G*) or silenced (*H*) C_2C_{12} cells exposed to DM for 48 h in control-transfected cells exposed to vehicle (white columns) and CB1 or CB1 siRNA-transfected cells in the presence of vehicle (0.1% DMSO, black columns) or ACEA (1 μM, gray columns). $^*P \leq 0.05$ vs. control-transfected C_2C_{12} cells. Data are means ± SEM of at least four separate experiments.

exposure to DM (2% HS) in the presence of ACEA (1 μM) or 2-AG (Fig. 4*F*). Conversely, both *MYOG* and *TNNT-1* mRNA expression was slightly increased in differentiating hSkMCs after 48 h of exposure to DM in the presence of 3 μM AM251 (Fig. 4*F*).

To further clarify the role played by CB1 during myotube formation, we transiently overexpressed the *CNR1* gene in C_2C_{12} myoblasts, and the day following the transfection we exposed the cells to DM for 2 d. After this incubation, qPCR analysis revealed that *Myog* and *Tnnt-1* mRNA levels were reduced by about 50% in differentiating C_2C_{12} cells overexpressing CB1 compared with control cells transfected with the empty plasmid (Fig. 4*G*). As predicted, in C_2C_{12} cells overexpressing CB1, the inhibitory effect of ACEA (1 μM) on *Myog* and *Tnnt-1* expression was stronger than that found in nontransfected or control plasmid-transfected cells (Fig. 4 *A* and *G*).

Next, we used also the opposite strategy of inducing post-transcriptional *Cnr1* gene silencing by using siRNA sequences. These were transfected into the myoblasts, and the day after the transfection, cells were exposed to DM for 48 h. Under these conditions, qPCR analysis could not detect any significant change in *Myog* and *Tnnt-1* expression in siRNA-*Cnr1* cells compared with control cells (transfected with scrambled siRNA sequences), although *Myog* expression showed a trend towards up-regulation (Fig. 4*H*). Importantly however, in CB1-silenced cells exposed to DM, the inhibitory effect of ACEA (1 μM) on *Myog* and *Tnnt-1* expression was completely lost, thus arguing strongly in favor of a CB1-mediated mechanism.

The selective CB2 receptor agonist JWH-133 (27) also reduced *Myog* mRNA expression at the dose of 3 μM. However, this effect was only partially reversed in the presence of the selective CB2 antagonist/inverse agonist AM630 (28), which per se (1 μM) did not change *Myog* mRNA expression (Fig. S3 *A* and *B*).

Thus, taking into consideration the *Cnr1* and *Cnr2* gene expression profiles and the pharmacological and biochemical evidence described so far, it appears that the ECS is regulated during myogenesis in a way such that CB1 receptor expression and stimulation exerts an inhibitory effect on the differentiation process in both murine C_2C_{12} cells and hSkMC.

Morphological Analysis of Myotube Formation During CB1 Stimulation in C_2C_{12} Cells. Given the above described inhibitory effects of CB1 stimulation on the expression of early markers of myogenesis (*Myog*, *Tnnt-1*), we carried out a morphological analysis to evaluate the effects of prolonged exposure to 2-AG and ACEA on myotube

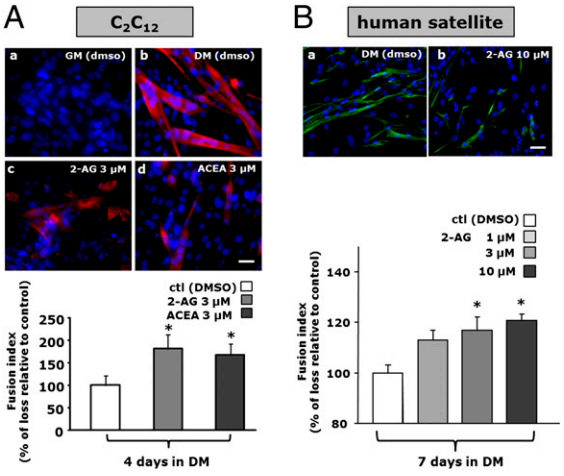

Fig. 5. Morphological analysis of myotube formation after ACEA and 2-AG exposure in murine C_2C_{12} and human primary satellite cells. (*A*) Immunofluorescence analysis of C_2C_{12} myoblasts exposed to DM for 4 d in the presence of vehicle (DMSO, control), 2-AG, or ACEA. MyHC (red) and DAPI (blue) in myoblasts (*a*) and in myotubes exposed to DMSO (*b*), 3 μM of 2-AG (*c*), and 3 μM of ACEA (*d*). (Scale bar, 10 μm.) The percentage of loss of polynucleated myotubes (fusion index) was calculated in both 2-AG– and ACEA-treated cells relative to the control-MyHC(+) myotubes (*Lower*). $^*P \leq 0.05$ vs. control-MyHC(+) cells. (*B*) Desmin immunofluorescence (green) and DAPI (blue) signal in control (*a*) or 2-AG–treated (*b*) human primary satellite cells differentiated for 7 d. The fusion index (*Lower*) was calculated in control (vehicle) and 2-AG–treated cells relative to control-desmin(+) cells. $^*P \leq 0.05$ vs. desmin(+) cells. Values are from independent fusion index measurements performed in 15 microscopic fields, randomly selected from four coverslips for each experimental condition (control or drug exposure).

formation by staining C_2C_{12} cells after 4 d of exposure to DM (± drugs) with an antibody directed against the MyHC protein. MyHC is a widely used marker of mature myotube formation (29). DAPI was also used to stain the nuclei. After 4 d of DM in the presence of vehicle (DMSO), myoblasts fused to form myotubes (Fig. 5 *A*, *a* and *b*). By contrast, when the DM contained 2-AG (3 μM) or ACEA (3 μM), myotube formation was strongly impeded as revealed by the decreased number and size of MyHC red-positive myotubes detected (Fig. 5 *A*, *c* and *d*). Quantification of these pharmacological effects, using the percentage of loss of fused polynucleated myotubes (fusion index), revealed a significant impairment in C_2C_{12} myotube formation with 2-AG or ACEA treatment (Fig. 5*A*, *Lower*).

Next, we investigated the 2-AG effect on primary satellite cells isolated from human muscle specimens from four different donors. Normally, 6–7 d of DM exposure represents the minimum period required to begin fusion in primary satellite cells, whereas at least 1 month is necessary to form mature myotubes (30). To evaluate the effect of 2-AG on the early phase of satellite cell differentiation, after 7 d of their exposure to DM, we evaluated the fusion index by staining the cells with an antibody against desmin, a canonical skeletal differentiation marker (30), and DAPI. We found that differentiating human satellite cells treated with 2-AG (1–10 μM), after 7 d of exposure to DM, exhibit a significant and dose-dependent decrease of fused, desmin-positive cells (Fig. 5*B*).

In an attempt to determine the relevance of CB1 to myogenesis in vivo, we examined the gastrocnemius muscles of *Cnr1*$^{-/-}$ mice at different developmental time points (Fig. 6). At E18, the number of MyHC fibrils per muscle fascicle was increased in *Cnr1*$^{-/-}$ mouse tissues. At this age, we also observed a coincident increase in the number of nuclei per primary fascicle (Fig. 6 *A*, *B*, *F1*, and *F2*), whereas the cross-sectional area of the individual fibers remained constant. However, the ratio between the number of nuclei and the number of muscle fibers per muscle fascicle (Fig. 6*F3*) remained unchanged between wild-type and *Cnr1*$^{-/-}$ mice. We suggest that these data provide genetic evidence of increased differentiation in topologically disorganized muscle fascicles with *Cnr1* deletion.

By P5, knockout of *Cnr1* was associated with a marked increase in *MyHC* and increased myofibril diameter, although not in the cross-sectional area (Fig. 6 *C* and *D*). Similar to the results of our analysis at E18, the muscle fiber/nucleus ratio in *Cnr1*$^{-/-}$ mice remained unchanged relative to wild-type littermates, suggesting a primary effect of the genetic manipulation on muscle differentiation rather than on cell proliferation (Fig. 6 *G1–G4*). The qPCR analysis of muscle samples at E18 and P5 confirmed the presence of *Cnr1* expression in wild-type controls and its absence in *Cnr1*$^{-/-}$ littermates. *Cnr2* levels remained unchanged.

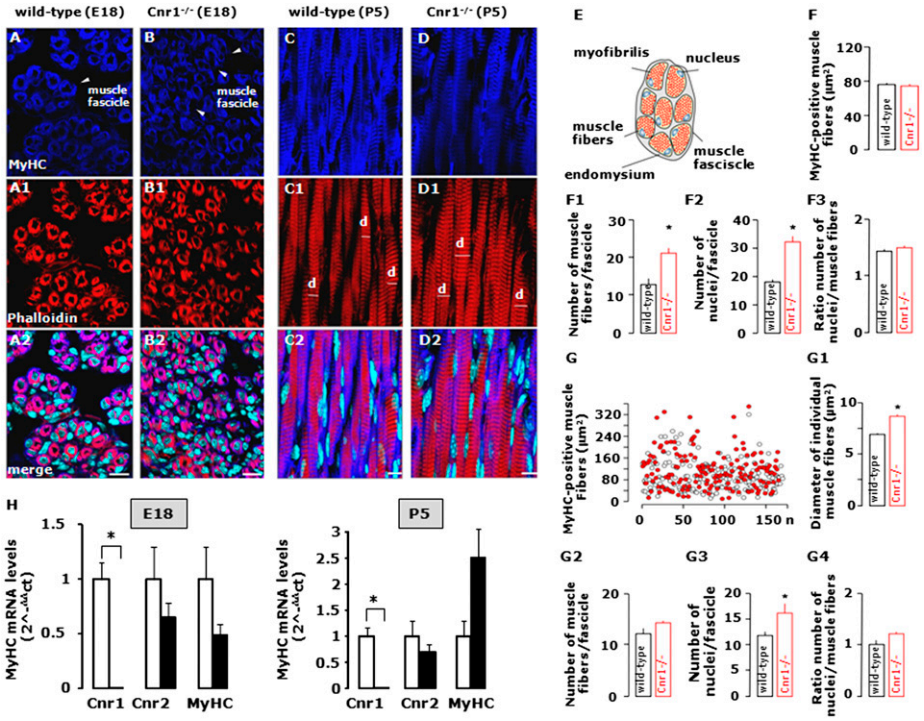

Fig. 6. Morphological analysis of skeletal muscle structure in *Cnr1*$^{-/-}$ mice. (*A–B2*) Cross-sections of the musculus gastrocnemius pars interna of E18 mouse embryos. Note that the diameter of individual muscle fibers was unchanged in *Cnr1*$^{-/-}$ (*B–B2*) mice relative to wild-type controls (*A–A2*). However, a striking difference in the anatomical organization of muscle fibers of *Cnr1*$^{-/-}$ mice was seen, compared with wild-type controls. (*C–D2*) Longitudinal sections of the gastrocnemius pars externa at P5. Note that the diameter of single fibers (d) is increased in *Cnr1*$^{-/-}$ mice (*D–D1*), compared with wild-type controls (*C–C1*). (*E*) Schematic representation of the cellular components and organization of muscle fascicles. (*F–F3*) In E18 embryos, the area of MyHC-positive muscle fibers was not significantly changed in *Cnr1*$^{-/-}$ mice, compared with wild-type controls (*F*). In contrast, a significantly increased number of muscle fibers (*F1*), as well as the density of nuclei, was observed (*F2*). Note that the ratio of number of nuclei per muscle fibers remained unchanged in *Cnr1*$^{-/-}$ mice relative to wild-type controls (*F3*). (*G*) Plotting of data from >150 muscle fibers/group showed that the surface area of MyHC-positive muscle fiber profiles from cross-sections in *Cnr1*$^{-/-}$ mice had a larger spread than in controls, suggesting the deregulation of fiber differentiation. (*G1*) More detailed analysis of the diameter of longitudinal muscle fibers (*C–D2*) revealed significantly increased diameter of individual longitudinal muscles fibers. (*G2–G4*) In P5 cross-sections (histochemical data not shown), the number of muscle fibers (*G2*) and nuclei (*G3*) per fascicle coincidently increased (reaching significance in *G3*). However, the ratio of these parameters remained unchanged (*G4*), suggesting the unlikely contribution of cell proliferation to the *Cnr1*$^{-/-}$ mice phenotype. Data were expressed as means ± SEM; **P* < 0.05. (Scale bar, 10 μm for *A2*, *B2*, *C2*, and *D2*). (*H*) MyHC mRNA expression levels in quadricipes femoris dissected from the mouse leg at E18 and P5. Each bar represents the mean ± SEM of at least three separate determinations. **P* < 0.05 vs. wild type.

The expression levels of the muscle marker MyHC showed no difference between wild-type and *Cnr1*$^{-/-}$ mice, although an increasing trend was observed at P5 in *Cnr1*$^{-/-}$ mice (Fig. 6*H*).

Pharmacological, Electrophysiological, and Biochemical Evidence for a PIP2-Mediated Functional Interaction Between CB1 Receptors and K_v7 Potassium Channels in C_2C_{12} Cells. Given that ion channels, and K^+ channels in particular, play a critical role in skeletal myogenesis, and in consideration of the permissive role in this process recently attributed to $K_v7.4$ channels (13, 14), we investigated the expression profile of both *Cnr1* and *$K_v7.4$* in vivo during muscle development. Toward this aim, we dissected the quadriceps femoris from mice at E18 and P4 and subjected them to qPCR analysis. We observed a robust increase in *MyHC* mRNA expression from E18 to P4, indicating increased muscle development. By P4, *Cnr1* transcript levels were decreased (about 50%) compared with embryonic expression, whereas, in contrast, muscle *$K_v7.4$* mRNA expression was increased by about 12-fold (Fig. S4). These data indicate that in vivo myogenesis is associated with a down-regulation of CB1 expression and an up-regulation of *$K_v7.4$*.

To explore the possible involvement of $K_v7.4$ channels in the antimyogenic effects of CB1 activation in C_2C_{12} myoblasts, a pharmacological approach was first used, in which C_2C_{12} cells were exposed to DM for 48 h in the absence or presence of the CB1 receptor agonist ACEA and the selective blocker of K_v7 channels XE991 (31); differentiation was assessed by qPCR quantification of myogenic marker transcript levels. When differentiating C_2C_{12} cells were exposed to either ACEA (3 μM) or XE991 (60 μM), the mRNA expression levels of *Myog* and *Tnnt-1* were similarly reduced by about 50% (Fig. S4). When the cells were exposed to the two drugs together, their effects were not additive ($P > 0.05$ vs. ACEA 3-μM group), thus arguing in favor of a common molecular mechanism of action for the two drugs (Fig. S4).

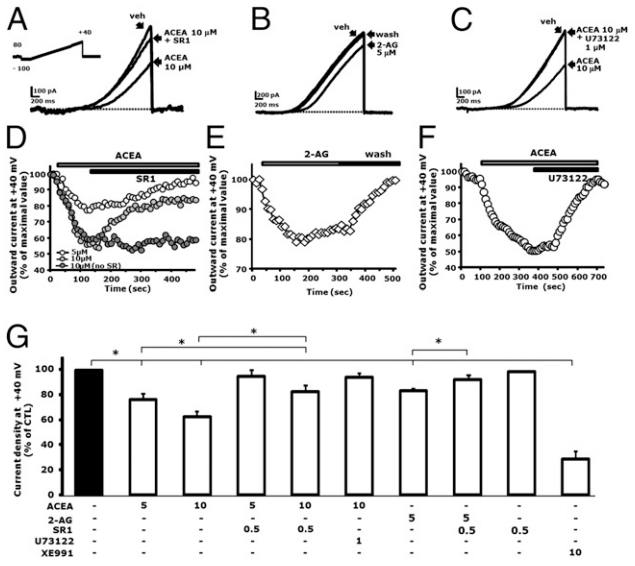

Fig. 7. CB1 receptor stimulation inhibits $K_v7.4$-mediated currents in CHO transfected cells. (*A*) Representative trace showing how ACEA in a concentration-dependent manner inhibits $K_v7.4$ currents. ACEA effect on $K_v7.4$ currents is prevented in the presence of (*A*) SR1 (0.5 μM) or (*C*) U73122 (1 μM). (*B*) Effect of 2-AG (5 μM). (*D*) Time course of the effects of ACEA (5 μM, white circles; 10 μM, light-gray circles) on $K_v7.4$ currents in CHO cells coexpressing CB1 receptors in the absence (dark-gray circle) or presence of 0.5 μM SR1 (white circle and light-gray circles). (*F*) Time course of the effects of ACEA (10 μM) on $K_v7.4$ currents in CHO cells coexpressing CB1 receptors in the absence or presence of 1 μM U73122. (*E*) Time course of the effects of 5 μM 2-AG on $K_v7.4$ currents in CHO cells coexpressing CB1 receptors. (*G*) Quantification of the experiments performed in this study. The length of the bars on top of the graphs indicate the duration of drug exposure. Asterisks denote values significantly different ($P < 0.05$) from the corresponding controls.

To gain direct evidence of the possible consequences of CB1 receptor activation on $K_v7.4$-mediated currents, we performed electrophysiological experiments in CHO cells transiently coexpressing both $K_v7.4$ channels and CB1 receptors. This strategy was chosen because the $K_v7.4$ currents could not be recorded in native C_2C_{12} cells (14). Bath application of ACEA (5 or 10 μM) caused a concentration-dependent inhibition of $K_v7.4$ currents (Fig. 7 *A* and *D*). During ACEA perfusion, the addition of the CB1 antagonist SR141716A (SR1; 0.5 μM) abolished the inhibition of $K_v7.4$ currents induced by the CB1 agonist (Fig. 7 *A* and *D*). Inhibition of $K_v7.4$ currents was also observed with the endocannabinoid 2-AG (5 μM) (Fig. 7 *B* and *E*), as well as with the classical K_v7 channel blocker XE991. PLC stimulation is a critical transduction mechanism triggered upon CB1 receptor activation in a variety of cell types (32–34). Treatment with the PLC inhibitor U73122 (1 μM) fully inhibited ACEA-induced inhibition of $K_v7.4$ currents [$K_v7.4$ current inhibition was 36 ± 5% in the presence of 10 μM ACEA ($n = 11$) and 6 ± 3% in the presence of ACEA plus U73122 ($n = 7$; $P < 0.05$)] (Fig. 7 *C* and *F*). Fig. 7*G* shows population data from a large number of cells studied under each experimental condition described; data are expressed as current density (pA/pF) relative to controls (DMSO). Altogether, these results suggest that, in a heterologous expression system, CB1 stimulation triggers PLC-mediated inhibition of $K_v7.4$ currents.

PIP2 levels are crucial regulators of K_v7 channels activity (19), and the activation of several receptors (muscarinic, in particular) is known to suppress K_v7 channel function by depleting membrane PIP2 levels. To test whether CB1 receptor activation also suppresses $K_v7.4$ currents by a PLC-dependent decrease in PIP2 levels, the endogenous levels of this phospholipid were measured by ELISA in C_2C_{12} myoblasts after 24 h of exposure to ACEA (1–3 μM). In this experiment, we decided to use undifferentiated cells to avoid the potentially confounding effects due to ACEA-induced inhibition of cell differentiation. As shown in Fig. 8*A*, ACEA significantly decreased PIP2 levels by about 30–40% in C_2C_{12} myoblasts. The effect of ACEA (1–3 μM) on PIP2 levels was also evaluated by measuring the signal intensity of the green fluorescent Bodipy-FL PIP2. In these experiments, the Bodipy-FL-PIP2 was first conjugated with the Shuttle PIP carrier and then added to the cells in serum-free medium for 10–15 min to allow its incorporation into the cell (see *Materials and Methods*). As shown in Fig. 8*B*, in myoblasts exposed to the vehicle (DMSO), Bodipy-FL-PIP2 produces a strong green fluorescent signal, which was markedly reduced following 5–10 min of ACEA (1–3 μM) exposure. The effect of ACEA was quantified by measuring the fluorescence intensity signal in randomly selected cell groups under each experimental condition (Fig. 8*B*, *Lower*). Finally, to gain conclusive evidence of a CB1-sensitive association between PIP2 and K_v7 channels, we exposed C_2C_{12} myoblasts for 24 h to ACEA or vehicle and then assayed $K_v7.4$ coimmunoprecipitated PIP2 levels. ACEA (1 and 3 μM) caused a robust reduction of coimmunoprecipitated PIP2, whereas $K_v7.4$ expression was unchanged (Fig. 8*C*). Carbachol (10 μM), a canonical agonist of G_q-coupled muscarinic receptors used as a positive control, caused a similar effect. In conclusion, these findings clearly support the idea that the inhibitory effect of CB1 receptor activation on myogenesis is largely dependent on the inhibition of $K_v7.4$ activity through G_q/PLC-mediated PIP2 hydrolysis.

Effect of 2-AG and ACEA on C_2C_{12} Myoblast Proliferation. Finally, to show that the increased number of fibers and nuclei per fascicle observed in the muscle of *Cnr1*$^{-/-}$ mice was not due to a negative effect of CB1 tone on myoblast proliferation, as suggested by the fact that the ratio between nuclei and muscle fiber was not altered in these mice, we investigated the effect of CB1 activation

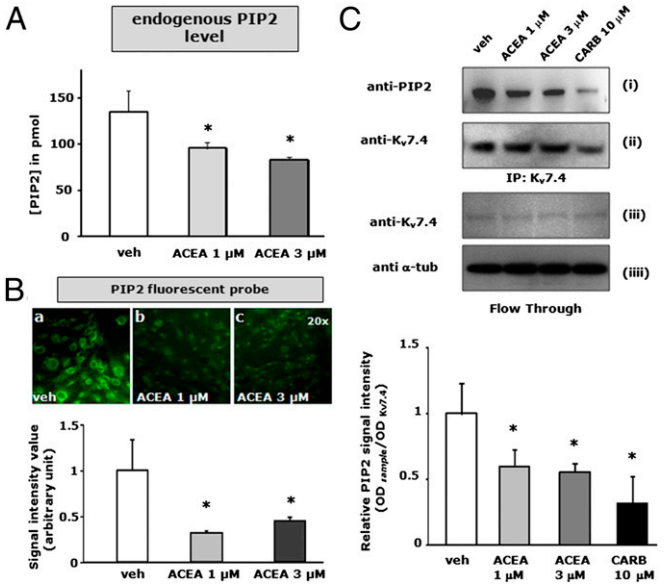

Fig. 8. CB1 stimulation by ACEA reduces endogenous PIP2 levels and BODY-PY PIP2 fluorescence and PIP2 binding to $K_v7.4$ K^+ channels in C_2C_{12} myoblasts. (*A*) Endogenous levels of PIP2 quantified by ELISA in control (DMSO) and treated cells after 24 h of exposure to ACEA (1 and 3 μM) in GM. Each bar represents the mean ± SEM of three to four separate determinations performed in quadruplicate. *$P < 0.05$ vs. control (no drug added). (*B*) C_2C_{12} myoblasts incubated with BODY-PY PIP2 showing a green fluorescent signal in the control (DMSO) condition (*a*) and a robust decrease of signal after 5–10 min of exposure to 1 μM (*b*) or 3 μM (*c*) of ACEA. (*Lower*) The total signal intensity obtained arbitrarily by choosing four to six distinct preparations of cells. (*C, i*) The PIP2 signal in the immunoprecipitated samples for $K_v7.4$ (IP:$K_v7.4$) following the treatment with ACEA (1–3 μM) or carbachol (10 μM) by the use of a specific antibody (*Materials and Methods*). (*ii*) The $K_v7.4$ protein signal intensity on the same samples and membranes. (*iii* and *iiii*) The $K_v7.4$ and α-tubulin protein expression in the flow-through sample under each condition. The graph bar indicates the PIP2 band intensity value normalized to the relative amount of $K_v7.4$ in each condition.

on myoblast proliferation in vitro. To this end, we plated and synchronized the myoblast cell cycle by exposing C_2C_{12} cells for 18–24 h to DM with low serum and then switching them to GM supplemented with [^{3}H]thymidine in the absence or presence of drugs for a further 24 h to measure the effects on proliferation rate. As shown in Fig. 9, 2-AG (1 μM) and ACEA (1–3 μM) increased myoblast proliferation by about 30–40%. This proproliferative effect was counteracted by SR141716 (0.6 μM). By contrast, when myoblasts were exposed to a higher concentration of SR141716 (1 μM), proliferation was reduced (Fig. 9).

We next evaluated if the proproliferative effect of ACEA was still present when the compound was given to cells in combination with pertussis toxin (PTX) or D609, selective blockers of $G_{i/o}$ and PLC, respectively (35, 36). Interestingly, D609 (40 μM), but not PTX (500 ng/mL), significantly counteracted ACEA-induced proliferation of C_2C_{12} cells, thus suggesting that the proproliferative effect observed upon CB1 stimulation, like the differentiation-restricting effect described above, might be due to a G_q/PLC-mediated mechanism. D609 as well as PTX, when given alone, did not affect myoblast proliferation (Fig. 9). [^{3}H]Thymidine incorporation was lowest in those cells where the DM, after the cell cycle synchronization time, was not replaced with fresh GM (Fig. 9). In conclusion, CB1 receptor stimulation increases the number of precursor myoblasts in vitro in a PLC-dependent manner.

Discussion

EC Signaling Is Altered During Myogenesis in Vitro and in Vivo. During the early phases of skeletal muscle formation myoblasts withdraw from the cell cycle and fuse to form large and multinucleated myotubes, which represent the functional contractile unit in the mature myofiber (8). During this transition the coordinated action of a large number of genes including those encoding for transcriptional factors, metabolic enzymes, ion channels, and receptors, is required. In this study, we described, to our knowledge for the first time, that the ECS, which plays an important role in many physiological and pathological aspects of mammalian biology, participates also in myogenesis. To define the potential functional role played by the ECS during the early phases of skeletal muscle formation, we used murine C_2C_{12} cells as a model of myogenesis in vitro. AEA and 2-AG levels were measured during the myoblast–myotube transition, and a transcriptomic analysis of genes known to regulate EC metabolism and activity was performed. Our data show that 2-AG, but not AEA, levels significantly decline during C_2C_{12} myotube formation in vitro and during muscle formation in vivo. In myoblasts this might be due to an increase in MAGL expression and subsequent increased 2-AG enzymatic hydrolysis. During myoblast differentiation, we also found significant increases in the expression of both CB1 and CB2 receptors, with CB1 showing the strongest degree of up-regulation within the first 24–48 h of differentiation. Interestingly, the early phase of human primary myoblast differentiation was accompanied by CB1, but not CB2, up-regulation. Importantly, sufficient expression of CB1 mRNA and protein seems to occur also in both murine and human myoblasts, thus allowing for a possible modulation by the ECS of the early steps of myogenesis and suggesting pharmacological experiments in this direction.

Functional Role of the ECS During Skeletal Muscle Proliferation and Differentiation. We next investigated the possible function of the observed changes in EC levels and of CB1 and CB2 gene expression by pharmacological and biochemical approaches. To increase the levels of both AEA and 2-AG during the early phase of C_2C_{12} cell differentiation and study the potential effects on myogenesis, we used both exogenous EC and selective inhibitors of

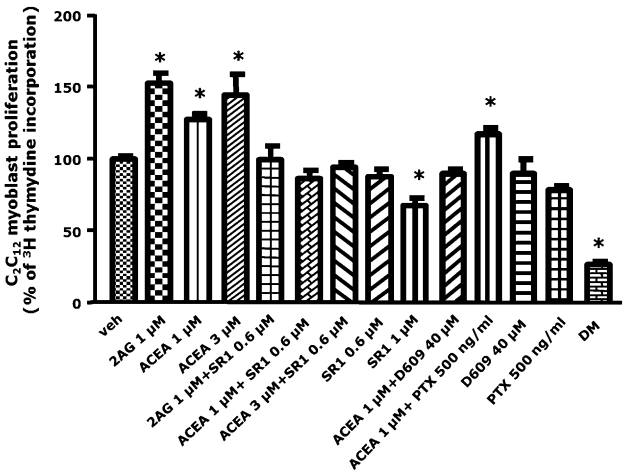

Fig. 9. Effect of 2-AG and ACEA on C_2C_{12} cell proliferation. C_2C_{12} myoblasts were synchronized by exposure to DM for 18–20 h; after this period, cell proliferation was assessed by [^{3}H]thymidine incorporation into cells grown for a further 24 h in GM (with or without the indicated drugs). Each point represents the mean ± SEM of three to four separate determinations performed in quadruplicate. *$P < 0.05$ vs. GM controls (no drug added). DM served as control condition as it represents the group of cells in which the DM was not refreshed with the GM after the starvation time of 18–20 h.

FAAH and MAGL. We found that 2-AG, but not AEA, inhibits myotube formation. A similar effect was found following exposure of differentiating C_2C_{12} cells to the selective synthetic CB1 agonist ACEA, which markedly reduced the expression of skeletal muscle differentiation markers (*Myog* and *Tnnt-1*) in a dose- and time-dependent manner and in a way antagonized by per se inactive doses of two selective CB1 blockers. These latter compounds, when given to cells at higher doses, as well as an inhibitor of 2-AG biosynthesis, instead increased *Myog* and *Tnnt-1* expression. These data, together with the above finding that endogenous 2-AG is produced in higher amounts in myoblasts and that an inhibitor of 2-AG degradation also counteracted myogenesis, suggest that this EC exerts a tonic negative control on myogenesis by activating CB1 receptors and that such control is released to allow myogenesis by increasing the expression of the 2-AG–inactivating enzyme. On the other hand, the up-regulation of CB1 expression immediately after the start of differentiation can be seen as a potential way of compensating for the decreased levels of 2-AG and allowing for a negative feedback control of myogenesis. This hypothesis is supported by our observation that overexpression of CB1 inhibited C_2C_{12} cell differentiation and heightened the inhibitory effect of ACEA, which instead was abolished by CB1 receptor knockdown. On the other hand, experiments with pharmacological tools selective for CB2, together with the much lower up-regulation of the latter during myogenesis, seem to rule out an important effect for this 2-AG target in myotube formation. Importantly, CB1 negative control of differentiation was observed also when using primary human myoblasts. Furthermore, when differentiation was carried out starting from human satellite skeletal muscle cells from healthy donors, 2-AG was again capable of inhibiting differentiation.

Finally, immunohistochemical and morphological analyses of skeletal muscle from CB1 null mice at E18 and P5, confirmed that CB1 receptors clearly play a role in inhibiting myotube differentiation and muscle formation also in vivo. In fact, during muscle development, both the number of fibers and nuclei in each fascicle were increased in the absence of CB1. Two lines of evidence indicate that this morphological observation can be explained with stimulation of myoblast differentiation rather proliferation by CB1 knockout. First, the ratio between nuclei and fibers in CB1 null mice at both E18 and P5 remained constant. Second, and most importantly, we found that, in vitro, CB1 antagonism, rather than enhancing, in fact reduces (whereas CB1 agonism enhances) C_2C_{12} myoblast proliferation, an effect that might be a mere consequence of the effect on differentiation shown here, as observed for CB1 in many cell types including neuronal stem cells, adipocytes, osteoblasts, smooth-muscle cells, etc. (37–39), and not necessarily occurring in vivo. Thus, it is likely that the observed increase in fiber number in CB1 null mice is due to the absence of 2-AG/CB1 negative control over satellite cell differentiation into myoblasts (Fig. 5*B*) and over myoblast differentiation into myotubes (Fig. 4), rather than to the absence of a negative control on myoblast proliferation. Such effects would be sufficient to sustain an increased muscle formation even in the absence of direct effects on myoblast proliferation.

In C_2C_{12} Cells, CB1 Stimulation Causes PIP2 Hydrolysis. We next investigated the molecular mechanism(s) through which CB1 controls myoblast proliferation and differentiation. CB1 belongs to the metabotropic class of receptors and, although prevalently coupled to $G_{i/o}$ proteins, it can also trigger $G_{q/11}$ activation and subsequent PLC activation (32–34, 40). Indeed, we provided evidence that, in C_2C_{12} cells, ACEA reduces the endogenous levels of the PLC substrate, PIP2. We surmise that, in differentiating myoblasts, CB1 activation leads to the activation of PLC and the subsequent hydrolysis of PIP2. Accordingly, we showed that the proproliferative effect produced by ACEA on C_2C_{12} myoblasts is abolished by a PLC inhibitor, but not by PTX. CB1-induced PIP2 hydrolysis might also release channels involved in differentiation from the positive control that PIP2 usually exerts thereupon and, at the same time, lead to the formation of diacylglycerols and IP3, with subsequent activation of protein kinase C and intracellular calcium mobilization, all of which have been implicated in both cell differentiation and proliferation (41, 42).

CB1 Receptor Activation-Induced PIP2 Hydrolysis Leads to Reduced Function of K_v7 Potassium Channels. K_v7 represents a subclass of K^+ channels comprised of five distinct members ($K_v7.1$– $K_v7.5$), each showing distinct subcellular localization, biophysical properties, modulation, and pharmacological profile (43). $K_v7.1$ subunits, together with the auxiliary subunits KCNE1, form the molecular basis of delayed rectifier K^+ currents, which control action potential repolarization in cardiomyocytes, whereas $K_v7.2$, $K_v7.3$, $K_v7.4$, and $K_v7.5$ give rise to K^+ currents (such as the M current) widely distributed in neuronal and primary sensory cells and acting as primary regulators of the intrinsic electrical properties of excitable cells (44). To date, the spectrum of functions attributed to K_v7 subunits has been enlarged following their description in smooth muscle cells of vascular and visceral tissues and in skeletal muscle cells. In this context, we recently showed that significant changes in the expression levels of some members of the K_v7 subclass of voltage-gated K^+ channels, most notably $K_v7.4$, accompany the myoblast-to-myotube transition in murine C_2C_{12} cells (14).

Over the past decade, many studies have described how the decrease of membrane PIP2 concentrations represents one of the main molecular mechanisms by which $G_{q/11}$-coupled metabotropic receptors inhibit the activity of K_v7 channels. Moreover, K_v7 channel open state probability also depends on its intrinsic affinity for intracellular PIP2 (45), with higher PIP2 concentrations increasing the open state probability of K_v7 channels. In view of the present data showing that CB1 stimulation in C_2C_{12} cells reduces differentiation and stimulates proliferation—i.e., two effects that are opposite to those observed following activation of K_v7 channels (13)—we hypothesized that CB1 receptor stimulation, by reducing PIP2 levels, might indirectly inhibit K_v7 channels. By using selective pharmacological tools and biochemical and electrophysiological approaches, we have provided strong evidence in favor of this hypothesis. In fact, we showed that CB1 stimulation reduces (*i*) the $K_v7.4$-mediated K^+ current in a PLC-dependent manner in CHO cells heterologously expressing CB1 and $K_v7.4$, but not in cells expressing only $K_v7.4$, and (*ii*) the amounts of PIP2 associated with $K_v7.4$ channels. We also investigated the potential effect of CB1 stimulation by ACEA on the IP3-dependent intracellular Ca^{2+} mobilization, an event also known to be coupled to inhibition and stimulation of myoblast differentiation and proliferation, respectively (46). However, in FURA-2:00 AM-labeled C_2C_{12} myoblasts exposed to DM for 24 h in a Ca^{2+}-free buffer, we could observe only a slight increase of $[Ca^{2+}]_i$ in response to ACEA. Interestingly, the M1 muscarinic receptor (but not the B2 bradykinin receptor) also was reported to inhibit K_v7 in the brain in a manner similar to that observed here in myoblasts for CB1—i.e., by decreasing PIP2 binding to the channel, rather than by increasing $[Ca^{2+}]_i$ and leading to calmodulin activation (15). The role of diacylglycerol and protein kinase C in CB1-mediated inhibition of $K_v7.4$ might therefore be an interesting subject of investigation for future studies in myoblasts.

Conclusions. The present study suggests that 2-AG, via CB1 activation, plays a crucial role in the control of myotube formation, and highlights $K_v7.4$ potassium channels as one important downstream target for this function. The novel molecular mechanism described here could open new avenues for the development of endocannabinoid-based therapies against skeletal muscle diseases characterized by abnormal repair and differentiation.

Materials and Methods

Cell Culture and Drugs. C_2C_{12} myoblasts were cultured and differentiated as previously described (13) (*SI Materials and Methods*). Satellite cells were obtained from muscle tissue from orthopedic surgery, as approved by the Ethical Committee of the University Medical School of Debrecen, and differentiated as previously described (30) (*SI Materials and Methods*).

Measurement of Endocannabinoids AEA and 2-AG. The extraction, purification, and quantification of EC from tissues was performed as previously described (47) (*SI Materials and Methods*).

Cell Transfection and *Cnr1* Gene Silencing and/or Overexpression. Myoblasts were plated in six-well culture dishes, and the next day, 4 μg of total DNA of pcDNA3.1-CNR1, or empty vector and a plasmid encoding for the enhanced green fluorescent protein (Clontech), was transfected using Lipofectamine LTX (Life Technologies) according to the manufacturer's instructions. The following day, C_2C_{12} myoblasts were exposed to DM for 48 h in the presence or absence of ACEA before RNA isolation and quantitation. *Cnr1* silencing was obtained by transfection of myoblasts plated in six-well culture dishes with endoribonuclease-prepared siRNA sequences (EMU088771 Sigma-Aldrich) using Lipofectamine RNAimax (Life Tecnology). The following day, the cells were exposed to DM for 48 h in the presence or absence of ACEA before RNA isolation and quantitation.

RNA Extraction and qPCR. Total RNA isolation, purification, and cDNA synthesis were performed as described (13) (*SI Materials and Methods*).

Cell Proliferation Assay. C_2C_{12} cell proliferation was assessed as previously described (13).

Western Blots. C_2C_{12} cells were subjected to Western blot analysis as described previously (13). For this study we used the following antibodies: mouse anti-myosin heavy chain antibody, clone A4.1025 (1:1,000; Millipore); mouse anti-CNR1 (1:500; catalog no. Y080037, Applied Biological Materials Inc.); mouse anti-CNR2 (1:400; Sigma-Aldrich); mouse anti-MGL clone N90/20 (1:4; Antibodies Inc.); and goat anti-DAGLα lot (1:1,000; Abnova). An anti–α-tubulin antibody (1:5,000; Sigma-Aldrich) was used to check for equal protein loading. Reactive bands were detected by chemiluminescence (ECL or ECL-plus; Bio-Rad). Images were analyzed on a ChemiDoc station with Quantity-one software (Bio-Rad).

Cell or Tissue Morphological Analysis. Murine C_2C_{12} cells were stained as previously described (14). Primary human muscle cells were stained as previously described (30). Heterozygous crosses of CB1RKO [$n = 3$ (E18), $n = 2$ (P5)] and wild-type littermates [$n = 3$ (E18), $n = 2$ (P5)] on C57Bl5/N background were processed simultaneously. In brief, embryos were harvested on E18, and the right hind paw was isolated and immersion-fixed for 48 h. Pups were decapitated on postnatal day 5 with the right hind paw processed as above. Subsequently, tissues were cryoprotected in 30% (wt/vol) sucrose in physiological saline and sectioned at a thickness of 14 μm on a cryostat microtome (Leica). The cutting plane was perpendicular to the musculus gastrocnemius pars externa (Fig. 6 *A* and *B*) and, consequently, parallel to the musculus gastrocnemius pars interna (Fig. 6 *C* and *D*). Serial sections were collected on fluorescence-free SuperFrost$^+$ glass slides, air-dried, and processed for multiple labeling histochemistry according to standard protocols (48) using a mouse anti-heavy chain myelin antibody (1:500, Millipore) antibody, Alexa560-conjugated phalloidin to reveal filamentous actin, and Hoechst 33,342 as nuclear dye. Imaging was performed on a Zeiss780 laser-scanning microscope using spectral detection for the optimal separation of fluorescence signals. Quantitative morphometry included (*i*) measurement of the cross-sectional surface of individual muscle fibers (μm^2) (Fig. 6 *A*, *B*, *F*, and *G*), determining (*ii*) the number of muscle fibers (Fig. 6 *F1–G2*) and the number of nuclei (Fig. 6 *F2–G3*) within primary muscle fascicles at both ages. Moreover, we measured the cross-sectional diameter (Fig. 6*G1*) of muscle fibers on P5. Data were expressed as means ± SEM; $*P < 0.05$.

ELISA and BODY-PY PIP2. The amount of PIP2 extracted from C_2C_{12} cells was measured by using the PIP2 Mass ELISA kit following the manufacturer's instructions (Echelon Biosciences Inc.). PIP2 was extracted from control or ACEA-treated cells (1–3 μM) after 24 h of drug exposure in GM. Cellular PIP2 quantities were estimated by comparing the values from the standard curve, which showed a linear relationship at the range from 0.5 to 1,000 pM concentration. Data were analyzed and graphed by using Graph-prism 5 software. The BODY-PY green fluorescent PIP2 (catalog no. C-45F6) as well as the shuttle carrier (catalog no. P-9045) were purchased from Echelon Biosciences Inc.

Immunoprecipitation. C_2C_{12} myoblasts were plated on 100-mm-diameter petri dishes and exposed to GM in the presence of vehicle (DMSO) or ACEA (1–3 μM) and carbachol (10 μM) for 24 h. After this time, the cells were washed twice in PBS (without Mg^{2+} and Ca^{2+}) and lysed in a buffer solution (Tris·HCl 50 mM, NaCl 150 mM, 1% Triton X-100, EDTA 2 mM, EGTA 5 mM, and protease inhibitors mixture). Total lysates were collected and maintained under agitation for 30 min at 4 °C before centrifugation for 15 min at 15,000 × *g*. Supernatants were recovered and quantified by a Bio-Rad DC Protein Assay Kit. Subsequently, 0.8–1 mg of each lysate sample was used for the immunoprecipitation (IP) procedure using a Dynabeads Protein G Kit (catalog no. 10007D; Life Technology) following the manufacturer's instructions. Mouse anti-K_v7.4 (IgG1) (catalog no. 75–082, Antibodies Inc.) was used to immunoprepitate K_v7.4 channels. IP samples were recovered after heating at 100 °C for 10 min in β-mercaptoetanol sample buffer (2×) and loaded on precast polyacrylamide gels (4–12% gradient; Bolt Bis-Tris Plus gels; Life Technologies) and then transferred to a PVDF membrane. Mouse anti-PIP2 antibody (1:1,000; catalog no. sc-53412, Santa Cruz Biotechnology) was incubated overnight at 4 °C. All of the proteins not pulled down by the anti-K_v7.4 antibody/beads complex (flow-through) were loaded (at a concentration of 50 μg) on precast polyacrylamide gels mentioned before and blotted using anti-K_v7.4 and anti–α-tubulin (1:500; Sigma-Aldrich) antibodies to verify the IP procedure.

Whole-Cell Electrophysiology. Currents from transiently transfected CHO cells (1 d posttransfection) were recorded at room temperature by whole-cell patch-clamp using an Axopatch 200A amplifier (Molecular Devices) with glass micropipettes of 3–5 MΩ resistance. The extracellular solution contained (in mM): 138 NaCl, 2 CaCl2, 5.4 KCl, 1 MgCl2, 10 glucose, and 10 Hepes (pH 7.4) with NaOH. The pipette (intracellular) solution contained (in mM): 140 KCl, 2 $MgCl_2$, 10 EGTA, 10 Hepes, 5 Mg-ATP (pH 7.4) with KOH. The pCLAMP software (version 10.2; Molecular Devices) was used for data acquisition and analysis. Linear cell capacitance (C) was determined by integrating the area under the whole-cell capacity transient, evoked by short (5–10 ms) pulses from −80 to −75 mV with the whole-cell capacitance compensation circuit of the Axopatch 200A turned off. Current densities (expressed in pA/pF) were calculated as peak of the agonist-evoked currents divided by C. From a holding potential of −80 mV, currents were activated by 4-s square pulses from −100 to +40 mV in 20 mV increments, followed by a 4-s isopotential pulse to 0 mV, or by using voltage ramps in which the membrane voltage was changed from −100 to +40 mV in 3 s.

Data Analysis. Data are expressed as means ± SEM of the given number of experiments (*n*). Data sets were compared by use of unpaired Student *t* tests or, if necessary, with one-way analysis of variance, followed by the Bonferroni's test using GraphPad Prism 5 software. Statistically significant differences were accepted when the *P* value was at least <0.05. The dose–response curves were calculated using GraphPad Prism 5 software.

ACKNOWLEDGMENTS. We thank Dr. Roberta Imperatore for help with the use of the fluorescent microscope, Dr. Roberta Verde and Dr. Teresa Aveta for lipid extraction, and Elisabeth Dögl and Joanne Bakker for great help with animal genotyping. This work was in part supported by Novo Nordisk Foundation (T.H.) and the Swedish Research Council (T.H.). D.C. is a recipient of a Karolinska Institutet–National Institutes of Health "Training Program in Neuroscience" grant.

1. Di Marzo V (2008) Targeting the endocannabinoid system: To enhance or reduce? *Nat Rev Drug Discov* 7(5):438–455.
2. Di Marzo V, Bisogno T, De Petrocellis L (2000) Endocannabinoids: New targets for drug development. *Curr Pharm Des* 6(13):1361–1380.
3. Rani Sagar D, Burston JJ, Woodhams SG, Chapman V (2012) Dynamic changes to the endocannabinoid system in models of chronic pain. *Philos Trans R Soc Lond B Biol Sci* 367(1607):3300–3311.
4. Smith PF (2005) Cannabinoids as potential anti-epileptic drugs. *Curr Opin Investig Drugs* 6(7):680–685.
5. Iannotti FA, et al. (2013) Analysis of the "endocannabinoidome" in peripheral tissues of obese Zucker rats. *Prostaglandins Leukot Essent Fatty Acids* 89(2-3):127–135.
6. Esposito I, et al. (2008) The cannabinoid CB1 receptor antagonist rimonabant stimulates 2-deoxyglucose uptake in skeletal muscle cells by regulating the expression of phosphatidylinositol-3-kinase. *Mol Pharmacol* 74(6):1678–1686.

7. Cavuoto P, McAinch AJ, Hatzinikolas G, Cameron-Smith D, Wittert GA (2007) Effects of cannabinoid receptors on skeletal muscle oxidative pathways. *Mol Cell Endocrinol* 267(1-2):63–69.
8. Walsh K, Perlman H (1997) Cell cycle exit upon myogenic differentiation. *Curr Opin Genet Dev* 7(5):597–602.
9. Bijlenga P, et al. (1998) An ether -à-go-go K+ current, Ih-eag, contributes to the hyperpolarization of human fusion-competent myoblasts. *J Physiol* 512(Pt 2):317–323.
10. Fischer-Lougheed J, et al. (2001) Human myoblast fusion requires expression of functional inward rectifier Kir2.1 channels. *J Cell Biol* 153(4):677–686.
11. Bijlenga P, et al. (2000) T-type alpha 1H Ca2+ channels are involved in Ca2+ signaling during terminal differentiation (fusion) of human myoblasts. *Proc Natl Acad Sci USA* 97(13):7627–7632.
12. Roura-Ferrer M, Solé L, Martínez-Mármol R, Villalonga N, Felipe A (2008) Skeletal muscle K_v7 (KCNQ) channels in myoblast differentiation and proliferation. *Biochem Biophys Res Commun* 369(4):1094–1097.
13. Iannotti FA, et al. (2010) Expression, localization, and pharmacological role of K_v7 potassium channels in skeletal muscle proliferation, differentiation, and survival after myotoxic insults. *J Pharmacol Exp Ther* 332(3):811–820.
14. Iannotti FA, Barrese V, Formisano L, Miceli F, Taglialatela M (2013) Specification of skeletal muscle differentiation by repressor element-1 silencing transcription factor (REST)-regulated $K_v7.4$ potassium channels. *Mol Biol Cell* 24(3):274–284.
15. Brown DA, Adams PR (1980) Muscarinic suppression of a novel voltage-sensitive K+ current in a vertebrate neurone. *Nature* 283(5748):673–676.
16. Cruzblanca H, Koh DS, Hille B (1998) Bradykinin inhibits M current via phospholipase C and Ca2+ release from IP3-sensitive Ca2+ stores in rat sympathetic neurons. *Proc Natl Acad Sci USA* 95(12):7151–7156.
17. Colino A, Halliwell JV (1987) Differential modulation of three separate K-conductances in hippocampal CA1 neurons by serotonin. *Nature* 328(6125):73–77.
18. Moore SD, Madamba SG, Joëls M, Siggins GR (1988) Somatostatin augments the M-current in hippocampal neurons. *Science* 239(4837):278–280.
19. Suh BC, Hille B (2005) Regulation of ion channels by phosphatidylinositol 4,5-bisphosphate. *Curr Opin Neurobiol* 15(3):370–378.
20. Schweitzer P (2000) Cannabinoids decrease the K(+) M-current in hippocampal CA1 neurons. *J Neurosci* 20(1):51–58.
21. Lauckner JE, et al. (2008) GPR55 is a cannabinoid receptor that increases intracellular calcium and inhibits M current. *Proc Natl Acad Sci USA* 105(7):2699–2704.
22. Hanus L, et al. (2001) 2-arachidonyl glyceryl ether, an endogenous agonist of the cannabinoid CB1 receptor. *Proc Natl Acad Sci USA* 98(7):3662–3665.
23. Fezza F, et al. (2002) Noladin ether, a putative novel endocannabinoid: Inactivation mechanisms and a sensitive method for its quantification in rat tissues. *FEBS Lett* 513(2-3):294–298.
24. Hillard CJ, et al. (1999) Synthesis and characterization of potent and selective agonists of the neuronal cannabinoid receptor (CB1). *J Pharmacol Exp Ther* 289(3):1427–1433.
25. Rinaldi-Carmona M, et al. (1994) SR141716A, a potent and selective antagonist of the brain cannabinoid receptor. *FEBS Lett* 350(2-3):240–244.
26. Gatley SJ, et al. (1997) Binding of the non-classical cannabinoid CP 55,940, and the diarylpyrazole AM251 to rodent brain cannabinoid receptors. *Life Sci* 61(14): PL191–PL197.
27. Huffman JW, et al. (1999) 3-(1′,1′-Dimethylbutyl)-1-deoxy-delta8-THC and related compounds: Synthesis of selective ligands for the CB2 receptor. *Bioorg Med Chem* 7(12):2905–2914.
28. Ross RA, et al. (1999) Agonist-inverse agonist characterization at CB1 and CB2 cannabinoid receptors of L759633, L759656, and AM630. *Br J Pharmacol* 126(3):665–672.
29. Bennett AM, Tonks NK (1997) Regulation of distinct stages of skeletal muscle differentiation by mitogen-activated protein kinases. *Science* 278(5341):1288–1291.
30. Boczán J, Boros S, Mechler F, Kovács L, Bíró T (2000) Differential expressions of protein kinase C isozymes during proliferation and differentiation of human skeletal muscle cells in vitro. *Acta Neuropathol* 99(2):96–104.
31. Wang HS, Brown BS, McKinnon D, Cohen IS (2000) Molecular basis for differential sensitivity of KCNQ and I(Ks) channels to the cognitive enhancer XE991. *Mol Pharmacol* 57(6):1218–1223.
32. Hermann H, et al. (2003) Dual effect of cannabinoid CB1 receptor stimulation on a vanilloid VR1 receptor-mediated response. *Cell Mol Life Sci* 60(3):607–616.
33. Lauckner JE, Hille B, Mackie K (2005) The cannabinoid agonist WIN55,212-2 increases intracellular calcium via CB1 receptor coupling to Gq/11 G proteins. *Proc Natl Acad Sci USA* 102(52):19144–19149.
34. De Petrocellis L, et al. (2007) Mechanisms for the coupling of cannabinoid receptors to intracellular calcium mobilization in rat insulinoma beta-cells. *Exp Cell Res* 313(14): 2993–3004.
35. Marini P, et al. (2009) Cannabinoid CB1 receptor elevation of intracellular calcium in neuroblastoma SH-SY5Y cells: Interactions with muscarinic and delta-opioid receptors. *Biochim Biophys Acta* 1793(7):1289–303.
36. Murthy KS, Zhou H, Huang J, Pentyala SN (2004) Activation of PLC-delta1 by Gi/o-coupled receptor agonists. *Am J Physiol Cell Physiol* 287(6):C1679–C1687.
37. Maccarrone M, et al. (2003) The endocannabinoid system in human keratinocytes. Evidence that anandamide inhibits epidermaldifferentiation through CB1 receptor-dependent inhibition of protein kinase C, activation protein-1, and transglutaminase. *J Biol Chem* 278(36):33896–903.
38. Gary-Bobo M, et al. (2006) The cannabinoid CB1 receptor antagonist rimonabant (SR141716) inhibits cell proliferation and increases markers of adipocyte maturation in cultured mouse 3T3 F442A preadipocytes. *Mol Pharmacol* 69(2):471–478.
39. Ofek O, et al. (2006) Peripheral cannabinoid receptor, CB2, regulates bone mass. *Proc Natl Acad Sci USA* 103(3):696–701.
40. Turu G, Hunyady L (2010) Signal transduction of the CB1 cannabinoid receptor. *J Mol Endocrinol* 44(2):75–85.
41. Berridge MJ (2009) Inositol trisphosphate and calcium signalling mechanisms. *Biochim Biophys Acta* 1793(6):933–940.
42. Faenza I, et al. (2008) Nuclear phospholipase C beta1 and cellular differentiation. *Front Biosci* 13:2452–2463.
43. Soldovieri MV, Miceli F, Taglialatela M (2011) Driving with no brakes: Molecular pathophysiology of K_v7 potassium channels. *Physiology (Bethesda)* 26(5):365–376.
44. Miceli F, et al. (2011) The voltage-sensing domain of K(v)7.2 channels as a molecular target for epilepsy-causing mutations and anticonvulsants. *Front Pharmacol* 2:2.
45. Li Y, Gamper N, Hilgemann DW, Shapiro MS (2005) Regulation of K_v7 (KCNQ) K+ channel open probability by phosphatidylinositol 4,5-bisphosphate. *J Neurosci* 25(43): 9825–9835.
46. Carrasco MA, Jaimovich E, Kemmerling U, Hidalgo C (2004) Signal transduction and gene expression regulated by calcium release from internal stores in excitable cells. *Biol Res* 37(4):701–712.
47. Matias I, et al. (2008) Dysregulation of peripheral endocannabinoid levels in hyperglycemia and obesity: Effect of high fat diets. *Mol Cell Endocrinol* 286(1-2, Suppl 1): S66–S78.
48. Mulder J, et al. (2011) Molecular reorganization of endocannabinoid signalling in Alzheimer's disease. *Brain* 134(Pt 4):1041–1060.